Atomic disorder and superconductivity in $Ca_3Rh_4Sn_{13}$

1989 J. Phys.: Condens. Matter 1 5689

(http://iopscience.iop.org/0953-8984/1/33/012)

J. Phys.: Condens. Matter 1 (1989) 5689–5702. Printed in the UK

Atomic disorder and superconductivity in $Ca_3Rh_4Sn_{13}$

J P A Westerveld†, D M R Lo Cascio†, H Bakker†, B O Loopstra‡ and K Goubitz‡

† Natuurkundig Laboratorium, Universiteit van Amsterdam,. Valkenierstraat 65, 1018 XE, Amsterdam, The Netherlands

‡ Laboratorium voor Kristallografie, Universiteit van Amsterdam, Nieuwe Achtergracht 166, 1018 WV, Amsterdam, The Netherlands

Received 28 July 1988, in final form 8 February 1989

Abstract. Superconducting $Ca_3Rh_4Sn_{13}$ was quenched from high temperatures. X-ray diffraction measurements gave an indication of the type of defects (Sn atoms on the Ca sublattice) generated at high temperatures that are responsible for the degradation of the superconducting transition temperature. The relative degradation turns out to be about 10% for each per cent of anti-site Sn atoms on the Ca sublattice. Restoration of the superconducting transition temperature by annealing at intermediate temperatures is employed to study the kinetics of the defects. Values are obtained for the vacancy formation energy (1.10 eV) and the vacancy migration energy (0.89 eV). The activation energy for the annealing of anti-site defects is measured as 2.14 eV ($\simeq$1.10 eV + 0.89 eV), which suggests a vacancy mechanism for diffusion. The pre-exponential factor in the relaxation time for vacancy migration is obtained as 1.3×10^{-3} s and that for annihilation of anti-site atoms as 9.3×10^{-10} s.

1. Introduction

The compound $Ca_3Rh_4Sn_{13}$ is a member of the family of ternary rhodium stannides. Among these stannides, $Ca_3Rh_4Sn_{13}$ is the one with the highest superconducting transition temperature ($T_c = 8.6$ K). In the crystal structure of this compound the Sn atoms occupy two different sites: at one of the sites the atoms (Sn(I)) are anion-like, whereas at the other site (Sn(II)) they show a cation-like behaviour (Hodeau *et al* 1980, Rameika *et al* 1980). The unit cell of the structure contains two formula units: $Ca_6Sn(I)_2Rh_8Sn(II)_{24}$. The Sn(I) atoms together with the Ca atoms form a sublattice with the A15 structure. The A15 sublattice and the rhodium sublattice of the crystal structure are shown in figure 1. The Sn(II) atoms are omitted for reasons of clarity.

In a previous paper (Westerveld *et al* 1987) we described the strong T_c-dependence of $Ca_3Rh_4Sn_{13}$ and $Yb_3Rh_4Sn_{13}$ on the degree of atomic order. We assumed that the A15-sublattice $Ca_6Sn(I)_2$ was very important for the superconducting properties and that the atomic disorder mainly consists of anti-site defects in this A15 frame. This means that for each Sn atom situated on the Ca sublattice one Ca atom occupies a Sn(I) lattice position. We assumed that the degradation of T_c was caused by the atomic disorder that exists at high temperature and is frozen-in by rapid quenching to room temperature. The higher the quenching temperature, the higher the degree of atomic disorder and

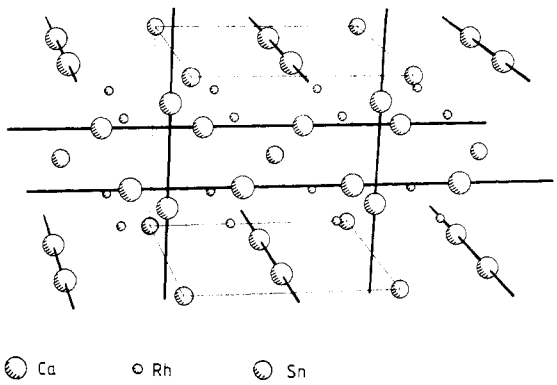

Figure 1. The Sn(I)–Ca_3 and Rh sublattices of the crystal structure of $Ca_3Rh_4Sn_{13}$. The Sn(I) atoms are located in the centre and on the corners of the primitive cell. The Ca atoms form linear 'chains' in the planes of the cube. The Rh atoms are located on the corners of a smaller cube with positions $(\frac{1}{4}\frac{1}{4}\frac{1}{4})$.

the lower the superconducting transition temperature. From theoretical considerations we expected an Arrhenius-type relation between the degradation of the superconducting transition temperature and the temperature from which the samples are quenched. This was confirmed by experiment. The activation energy appeared to be the same for both compounds, i.e. 1.16 eV (Westerveld *et al* 1987).

This behaviour was postulated in analogy to the A_3B intermetallic A15 compounds among which the conventional superconductors with the highest T_c are found. Here the long linear chains of A atoms, with A–A distances shorter than in the pure A metal, are thought to be responsible for the high T_c and to result in a high density of states at the Fermi level. Anti-site defects in these metallic systems induced by neutron irradiation or by quenching from high temperatures have been proved to cause a dramatic degradation of the superconducting transition temperature (Flükiger *et al* 1976).

In order to confirm that in the ternary compound anti-site disorder between the Sn(I) and the Ca sublattices really occurs and that this anti-site disorder is responsible for the T_c degradation we report on x-ray measurements of the sublattice occupancies. Furthermore, by annealing at intermediate temperatures we studied the recovery of the superconducting transition temperature after quenching to elucidate the defect kinetics.

2. Experimental procedure

The crystals of $Ca_3Rh_4Sn_{13}$ were grown in a molten metal solution of Sn with 3.01 at.% Ca and 3.34 at.% Rh. After slow cooling from 1050 °C down to 525 °C at a rate of 5 °C h^{-1}, the batch was held for 20 hours at this temperature before it was taken out of the furnace. The excess of tin solvent was removed by centrifuging the melt and dissolving the remaining film of Sn in hydrochloric acid. Powdered samples with grain sizes between 0.21 and 0.48 mm were used for the quenching experiments. For more details on sample preparation and quenching technique the reader is referred to a previous paper on the degradation of T_c upon quenching (Westerveld *et al* 1987).

One of the crystals from the batch was cleaved. One part was quenched from 835 °C. Both were polished and scanned under the electron microscope and the composition was simultaneously determined by microprobe analysis. These compositional analyses were performed on a Jeol 747 Superprobe at Eindhoven University of Technology, using the matrix correction program developed by Bastin *et al* (1984a,b). The chemical composition was measured at 200 points over a straight line of 1 mm length.

Table 1. Characterisation of the as-grown and the quenched sample of $Ca_3Rh_4Sn_{13}$.

	As-grown	Quenched $T_q = 835$ °C
a-axis (Å)	9.7239(3)	9.7202(2)
Space group (cubic)	Pm3*n*	Pm3*n*
Z	2	2
Crystal size (mm)	0.10 × 0.13 × 0.15	0.08 × 0.13 × 0.20
Min. Abs. Corr.	0.79	0.74
Max. Abs. Corr.	1.16	1.17

The x-ray measurements to determine the relative occupancies of the sublattices were performed on the quenched and as-grown samples. Neutron diffraction is less suitable than x-ray diffraction because of the small differences in scattering properties for neutrons between the Ca and Sn atoms and because of the large crystals needed for neutron diffraction.

Intensities were measured on an ENRAF-NONIUS CAD4 diffractometer using graphite-monochromated Mo Kα radiation ($\lambda = 0.71069$ Å). For the as-grown sample 1451 unique reflections ($1.1° < \theta < 65°$; $-14 \leq h \leq 0$; $0 \leq k \leq 17$; $1 \leq l \leq 24$) were collected. Cell parameters were refined by a least-squares fit, using 24 reflections with $41.8° < \theta < 44.8°$. Experimental data are given in table 1. Atomic parameters for Ca, Sn and Rh atoms were taken from Hodeau *et al* (1980), with Ca on the Yb position. Block-diagonal, least-squares refinement for 902 observed reflections ($F \geq 5\sigma_F$) with anisotropic temperature factors converged to $R = 0.030$ and $R_w = 0.018$, respectively. Extinction correction and an empirical absorption correction (DIFABS, see Walker and Stuart (1983)) were applied. The weighting scheme used was $w = 1/\sigma_{F_{obs}}$. The quenched sample was treated in the same way. Here, 1446 unique reflections were collected. Least-squares refinement was based on 968 observed reflections ($F \geq 5\sigma_F$) and converged to $R = 0.035$ and $R_w = 0.023$, respectively. Results are given in table 2.

Instead of refining the occupancy of the atomic sites, as done by Hodeau *et al* (1980), we integrated the electron density at the atomic sites from a F_{obs} synthesis. This procedure gives a quite stable result, while the refinement of occupancies leads to a very flat minimum and accordingly large uncertainties. The integration amounts to a summation of the electron density in the F_{obs}-synthesis at all grid points connected with a particular atomic site, multiplied by the volume of the grid cell. If the grid is sufficiently fine, a fairly accurate approximation of the number of electrons is obtained. From trials with different grids we found that the best result is obtained with an integration volume of $2 \times 2 \times 2$ Å^3 around an atomic site and a 0.1 Å grid interval. Results based on these parameters are listed in table 3 in § 3. All calculations were carried out with the XTAL system (Hall and Stewart (1987)).

The reordering experiments consisted of isochronal and isothermal annealing studies on powdered samples after quenching from high temperature. Most of these experiments were performed on grains from one single batch that were quenched from 810 °C. Before quenching the sample in water, it was kept at this temperature for about 70 minutes. To avoid compositional variations and a difference in heat treatment between the various grains, the grains were all quenched together. After quenching, the sintered grains were separated from each other by hydrochloric acid and the powder was divided into several

Table 2. Positional and thermal parameters for the as-grown and the quenched sample of $Ca_3Rh_4Sn_{13}$.

		Sn(2)	Ca(6)	Rh(8)	Sn(24)
As-grown	x	0	$\frac{1}{4}$	$\frac{1}{4}$	0
	y	0	$\frac{1}{2}$	$\frac{1}{4}$	0.30365(3)
	z	0	0	$\frac{1}{4}$	0.15340(3)
	U_{11}	0.0169(2)	0.0112(6)	0.0074(1)	0.0067(1)
	U_{22}	0.0169(2)	0.0095(3)	0.0074(1)	0.0281(1)
	U_{33}	0.0169(2)	0.0095(3)	0.0074(1)	0.0093(1)
	U_{12}	0	0	−0.0004(1)	0
	U_{13}	0	0	−0.0004(1)	0
	U_{23}	0	0	−0.0004(1)	0.0031(1)
Quenched	x	0	$\frac{1}{4}$	$\frac{1}{4}$	0
	y	0	$\frac{1}{2}$	$\frac{1}{4}$	0.30398(4)
	z	0	0	$\frac{1}{4}$	0.15355(3)
	U_{11}	0.0200(2)	0.0107(7)	0.0077(1)	0.0066(1)
	U_{22}	0.0200(2)	0.0101(4)	0.0077(1)	0.0231(2)
	U_{33}	0.0200(2)	0.0101(4)	0.0077(1)	0.0094(1)
	U_{12}	0	0	−0.0003(1)	0
	U_{13}	0	0	−0.0003(1)	0
	U_{23}	0	0	−0.0003(1)	0.0030(1)

portions, wrapped in tantalum foil and encapsulated in quartz tubes, which were evacuated before sealing. Annealing took place in Tempress diffusion furnaces, in which the temperature could be controlled within 1 °C and kept constant over a distance of about 50 cm. Superconducting transition temperatures were obtained by AC-susceptibility measurements at a frequency of 90 Hz. The superconducting transition temperature was taken as the temperature where the susceptibility becomes 'zero', the so-called onset-T_c. The recovery plots were determined for eight different annealing temperatures ranging from 280 °C to 460 °C with annealing times between 3 hours and 6 weeks. Isochronal annealing was studied for 15 temperatures ranging from 200 °C to 560 °C with an annealing time at each temperature of 18 hours. Differential thermal analyses with a heating rate of 10 K min^{-1} and Guinier-Lenné x-ray picture (16 K h^{-1}) were used to determine the melting temperature of $Ca_3Rh_4Sn_{13}$.

3. Experimental results

The Guinier-Lenné x-ray measurements resulted in a melting temperature of 937 °C which was in good agreement with DTA experiments where we obtained 934 °C. Microprobe analyses showed that the compositions of both samples were equal within experimental error. Compositional gradients were neither detected in the as-grown crystal nor in the sample quenched from 835 °C. The composition turned out to be a little off the stoichiometric, namely $Ca_{2.90}Rh_{3.99}Sn_{13.11}$, where the error is less than 0.3% for each atomic species. Because of the excess of Sn in comparison with the stoichiometric composition, 3.3% of the Ca(6) sites should be occupied by Sn.

Table 3. Number of electrons on each sublattice site in the as-grown and the quenched sample.

	Sn(2)	Ca(6)	Rh(8)	Sn(24)
As-grown	48.70	19.57	46.01	50.13
$T_q = 835\,°C$	47.12	20.12	45.45	50.31

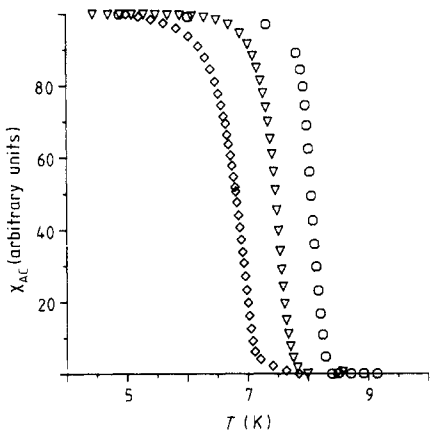

Figure 2. The AC susceptibility of $Ca_3Rh_4Sn_{13}$ versus the temperature. Open circles, as-grown; open diamonds, $T_q = 810\,°C$; open triangles, $T_a = 400\,°C$, 67 h.

X-rays were used to obtain the number of electrons per sublattice site for the as-grown sample and for the sample quenched from 835 °C. These data, given in table 3, are normalised to a mean value of 44.65 electrons per lattice site, as is to be expected from a chemical composition of $Ca_{2.90}Rh_{3.99}Sn_{13.11}$. Only small differences in the electron densities on the sublattices are found between the quenched and the as-grown samples. Although on the basis of the given numbers it is difficult to draw definite conclusions, considering the experimental uncertainties, the over-all picture is at least consistent with anti-site disorder between the Sn(2) and the Ca(6) sublattices. In fact it is not possible to assess reliable values for the experimental errors, although the differences in both the values for Rh(8) and Sn(24), respectively, give an estimate, because these values should be equal in both crystals. Table 3 gives an indication of a decrease of the number of electrons on the Sn(2) sublattice due to quenching and an increase of the number of electrons on the Ca(6) sublattice. If we ascribe these changes to induced anti-site defects, 1.8% of the Ca(6) sublattice sites are, in addition to the 3.3% in the as-grown sample, occupied by Sn at 835 °C. From table 3 we observe also that 5.3% of the Sn(2) sites are occupied by calcium atoms. Thus for each calcium atom jumped to the Sn(2) sublattice exactly one tin atom could have jumped to the Ca(6) sublattice.

In figure 2 three AC-susceptibility measurements of the superconducting transition are shown. The curve of the sample, quenched from 810 °C, remains almost parallel to the curve of the as-grown sample, but the transition is shifted to a lower temperature. This suggest that the defects introduced upon quenching are uniformly distributed in the grains. The onset of the transition has lost its sharpness, most probably caused by too low a quench rate in respect of the size of the lumps of sintered grains. This results in a somewhat decreasing number of defects towards the centres of the lumps. The point where the extrapolated vertical part of the χ curve intersects the temperature axis

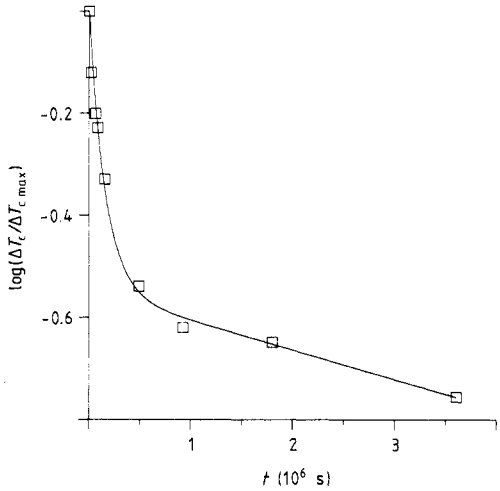

Figure 3. Isothermal annealing plot showing the logarithm of the recovery of the superconducting transition temperature $\Delta T_c/\Delta T_{cmax}$ versus the annealing time t in $Ca_3Rh_4Sn_{13}$. The annealing temperature is 280 °C.

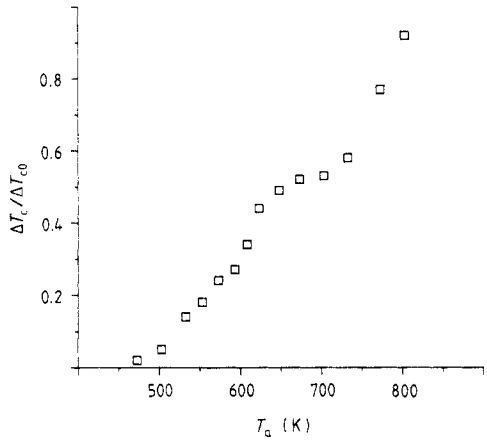

Figure 4. Isochronal annealing plot showing the recovery of the superconducting transition temperature $(T_c - T_{c0})/(T_{cmax} - T_{c0})$ versus the annealing temperature T_a in $Ca_3Rh_4Sn_{13}$. Annealing time is 18 h.

was taken as the onset transition temperature. After an annealing of 67 hours at a temperature of 400 °C half of the degradation of T_c is recovered as is shown in figure 2 by the inverted open triangles. A typical isothermal annealing plot is shown in figure 3. A very fast restoration of T_c is observed after short times. This can be attributed to the quenched-in excess of vacancies available in the first stage of the recovery process, which enhances the atomic jump rates. When the equilibrium concentration of vacancies is reached the restoration of T_c is much slower. Both stages in the recovery process can also be seen from the isochronal plot shown in figure 4. A plateau between the two stages is observed at 400 °C. After 18 hours at 530 °C the recovery of T_c (8.35 K) is almost complete.

To determine the vacancy formation enthalpy, three series of samples were quenched from different temperatures (780, 810 and 826 °C) and annealed at the same temperature of 320 °C. The higher the quenching temperature, the more vacancies are quenched in and the further is the relative recovery of T_c. As an example the annealing plots of the sample quenched from 780 °C and from 810 °C are given in figure 5. An example of quenching from the same temperature (810 °C), but annealing at different temperatures is shown in figure 6. Two isothermal plots with annealing temperatures of 300 °C and 350 °C are given in this figure.

The isothermal annealing curves will be analysed in terms of vacancy formation and vacancy mobility in relation to the anti-site reordering process in § 4 and § 5.

4. Theoretical framework

The following analysis is based on the results of the x-ray measurements that for the greater part anti-site defects are generated upon quenching and that only these defects have any influence on T_c. Besides, the jumping of the calcium and tin atoms from one

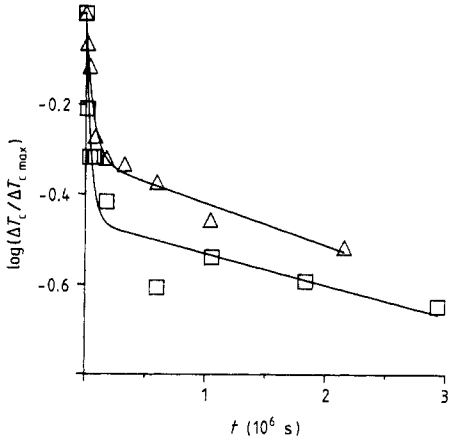

Figure 5. Isothermal annealing plot showing the logarithm of the recovery of the superconducting transition temperature $\Delta T_c/\Delta T_{cmax}$ versus the annealing time t in $Ca_3Rh_4Sn_{13}$. Open triangles, $T_q = 780\,°C$, $T_a = 320\,°C$; open squares, $T_q = 810\,°C$, $T_a = 320\,°C$.

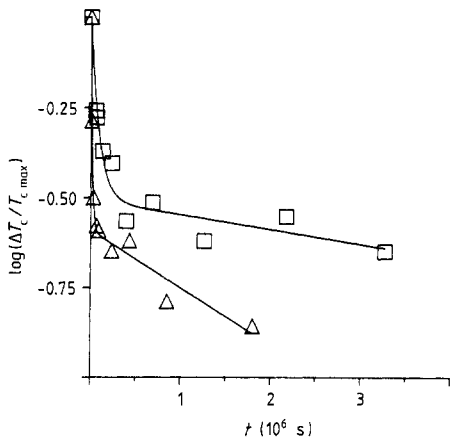

Figure 6. Isothermal annealing plot showing the logarithm of the recovery of the superconducting transition temperature $\Delta T_c/\Delta T_{cmax}$ versus the annealing time t in $Ca_3Rh_4Sn_{13}$. Open squares, $T_q = 810\,°C$, $T_a = 300\,°C$; open triangles, $T_q = 810\,°C$, $T_a = 350\,°C$.

sublattice to the other is assumed to take place via the usual 'vacancy mechanism'. This leads to two stages in the T_c recovery process. In the first stage the restoration is very fast because of the relatively large amount of vacancies present which enhances the atomic jump rate. The second stage starts when the excess of vacancies has disappeared and when the equilibrium annihilation rate of the anti-site defects has settled. Van Winkel *et al* (1985) did the same type of recovery measurements on the A15 compound V_3Ga, where both stages can also be distinguished. However, in V_3Ga a much smaller part of the recovery plot can be assigned to the first stage than in the present case, because of the much higher vacancy formation enthalpy in V_3Ga.

As mentioned above, two types of defects are frozen in when our material is quenched from high temperatures in water: anti-site defects and thermal vacancies. The equilibrium concentration of vacancies in a compound is temperature dependent. In pure metals we know that the vacancy concentrations are very low, even at the melting temperature. The expression for the vacancy fraction as a function of temperature is

$$c^v = \exp(-g^f_{1v}/kT) = \exp(s^f_{1v}/k)\exp(-h^f_{1v}/kT) \tag{1}$$

where g^f_{1v} is the Gibbs free energy for the formation of a monovacancy and s^f_{1v} and h^f_{1v} are the entropy and the enthalpy, respectively. For instance, a vacancy fraction of 10^{-4} at the melting temperature of 1234 K is to be expected for silver (Ag: $h^f_{1v} = 0.99$ eV, $s^f_{1v} = 0.5k$) (Franklin 1972). For pure tin a vacancy fraction of 3×10^{-5} at the melting temperature of 505 K, with $h^f_{1v} = 0.56$ eV and $s^f_{1v} = 2.52k$ is generally accepted.

In intermetallic compounds we have to specify the sublattice to which a vacancy fraction belongs. If the vacancies are formed on each sublattice in equal concentrations, i.e. following the chemical reaction:

$$20\mathrm{Vac}^g \rightleftharpoons \mathrm{Vac}^{\mathrm{Sn}(2)} + 3\mathrm{Vac}^{\mathrm{Ca}(6)} + 4\mathrm{Vac}^{\mathrm{Rh}(8)} + 12\mathrm{Vac}^{\mathrm{Sn}(24)} \tag{2}$$

where Vac^g is a lattice–gas vacancy and Vac^i is a vacancy on the ith sublattice, then we can handle the problem in terms of average vacancies with an average formation entropy

and enthalpy. Then the vacancy concentration on any of the sublattices is described by equation (1) as if we were dealing with a pure metal. However, the meaning of h^{f}_{1v} and s^{f}_{1v} are now the vacancy formation enthalpy and entropy averaged over the sublattices. This is identical to the situation of vacancy formation in, for example, NaCl and most probably V_2Ga_5 (Waegemaekers *et al* 1988). Let us try to estimate a value for this average vacancy formation enthalpy. In the same way as Bakker (1987) calculated the vacancy-formation enthalpy in the binary compounds using the Miedema model (Miedema and De Châtel 1979), we find for the three sublattices of the ternary $Ca_3Rh_4Sn_{13}$

$$h^{Ca}_{1v} = 0.86\ \text{eV} \qquad h^{Sn}_{1v}(\text{I}) = h^{Sn}_{1v}(\text{II}) = 0.87\ \text{eV} \qquad h^{Rh}_{1v} = 0.37\ \text{eV}$$

and the averge vacancy formation enthalpy $h^{f} = 0.77$ eV. This means that at a temperature of 800 °C we can expect 0.07% of the lattice-sites to be vacant.

The rate at which the excess of vacancies will disappear when the sample is annealed at low temperatures will depend on the diffusivity of the vacancies. The temperature dependence of the diffusivity is given by

$$D^{v} = D^{v}_{0} \exp(-h^{m}_{1v}/kT_a) \tag{3}$$

where D^{v}_{0} is the pre-exponential factor containing the entropy for vacancy migration, h^{m}_{1v} is the corresponding enthalpy, k the Boltzmann constant and T_a the annealing temperature. The excess of vacancies will decrease exponentially to zero by annihilation at sinks such as surfaces and dislocations:

$$\Delta c^{v}(t) = \Delta c^{v}(t = 0) \exp(-t/\tau^{v}) \tag{4}$$

with $\Delta c^{v}(t = 0)$ being the excess of vacancies at the start of the annealing experiment, t the annealing time and τ^{v} the relaxation time for the excess vacancy.

Also, to a first approximation, the excess of anti-site defects Δc^{α}_{B} will decrease exponentially if we assume this decrease to be of first order and if we assume constant vacancy concentration

$$\mathrm{d}(\Delta c^{\alpha}_{B})/\mathrm{d}t = \Delta c^{\alpha}_{B}/\tau^{a} \tag{5}$$

where τ^{a} is the characteristic relaxation time of the excess of anti-site defects. However, since an excess of quenched-in vacancies will also be present in the first stage of the annealing process of anti-site defects, τ^{a} turns out to be a function of annealing time: $\tau^{a}(t)$. The atomic diffusion coefficient is proportional to the vacancy content and so $\tau^{a}(t)$ will be proportional to the reciprocal concentration, so that

$$\tau^{a}(t = \infty)/\tau^{a}(t) = c^{v}(t)/c^{v}(t = \infty) \tag{6}$$

with $c^{v}(t)$ being the concentration of vacancies at time t of the annealing and $c^{v}(t = \infty)$ the equilibrium concentration of vacancies attained after infinitely long annealing times. After some algebra we obtain the solution of equation (5)

$$\ln(\Delta c^{\alpha}_{B}/\Delta c^{\alpha}_{B0}) = -(t/\tau^{a}) + (\Delta c^{v}(t = 0)/c^{v}(t = \infty))(\tau^{v}/\tau^{a})[\exp(-t/\tau^{v}) - 1] \tag{7}$$

where we define τ^{a} as $\tau^{a}(t = \infty)$.

For small concentrations of anti-site defects we showed in previous papers (Westerveld *et al* 1986, 1987) that the degradation of T_c is proportional to the concentration of anti-site defects

$$\Delta T_c/T_{cmax} = \text{const}\, c_B^{\alpha}. \tag{8}$$

Inserting equation (8) into (7) we obtain the final expression for the recovery of the superconducting transition temperature

$$\ln(\Delta T_c/\Delta T_{cmax}) = -(t/\tau^a) + (\Delta c^v(t=0)/c^v(t=\infty))(\tau^v/\tau^a)[\exp(-t/\tau^v) - 1]. \tag{9}$$

We will use this equation for analysing our experimental results and fitting our data. To visualise the parameters in equation (9) we refer to figure 3, where $1/\tau^a$ is the slope of the tail of the recovery curve, τ^v is the time after which the recovery process passes from stage 1 to stage 2 and where the intersection of the extrapolation of the tail of the curve with the vertical axis is given by

$$(\Delta c^v(t=0)/c^v(t=\infty))(\tau^v/\tau^a). \tag{10}$$

We will use the above equations for analysing our experimental results.

5. Discussion

First we will discuss the differences in the site occupancies as measured by x-rays and the implications for the dependence of T_c on atomic disorder. From the fact that we do not observe any change in composition after quenching and, moreover, that the recovery of T_c of quenched samples becomes complete after long annealing at intermediate temperatures, we conclude that the atomic defects induced at high temperatures are responsible for reversible changes in T_c. As mentioned before, only small changes in the site occupancies are found. The x-ray experiments turn out to be at least consistent with the concept of anti-site disorder generated at high temperatures. This behaviour is very similar to anti-site defects introduced by quenching in the A15 compound V_3Ga as observed by neutron diffraction (Flükiger *et al* 1976). Because of technical applications of the A15 materials in radiation fields many experiments have been performed on the influence of neutron irradiation on superconducting properties. Remarkably, the initial slopes of the depression of T_c with the neutron fluence appeared the same for different systems. For various A_3B A15 compounds (with the B element a non-transition metal) the slope of the degradation of T_c as a function of the neutron fluence is constant (Sweedler *et al* 1976) and is given by

$$\frac{d}{dt}\left(\frac{\Delta T_c}{T_{cmax}}\right) = 0.6 \times 10^{-19}\ \text{cm}^2/\text{n}. \tag{11}$$

Recovery experiments on irradiated samples show that T_c is strongly dependent on the concentration of anti-site defects and much less influenced by the presence of other defects, such as interstitials, for example. By the relation between the order parameter and the neutron fluence Fähnle (1982) was able to derive a general expression for the T_c degradation as a function of the concentration of anti-site defects in niobium A15 compounds

$$\Delta T_c/T_{cmax} = 26 c_B^{\alpha} \tag{12}$$

with c_B^{α} the fraction of B atoms on the chains and T_{cmax} the superconducting transition

temperature at $c_B^\alpha = 0$. However, in contrast to irradiation, quenching experiments from high temperatures have the advantage that the type of disorder is better defined and these experiments are therefore preferable for systematic defect studies. By quenching experiments, and subsequent neutron and x-ray diffraction studies on V_3Ga the concentration of anti-site defects in relation to T_c has been established by Flükiger *et al* (1976). By estimating the T_{cmax} of Flükiger's samples following Westerveld *et al* (1987) and using the experimental results of Flükiger *et al* (1976), it turns out that relation (12) is also obeyed in these quenching experiments within experimental error. This relation was also used by Van Winkel *et al* (1984) for the interpretation of quenching experiments on V_3Ga.

From the experiments we estimate the number of calcium atoms transferred to the Sn(2) sublattice, which is equal to number of Sn(I) atoms to the Ca(6) sublattice. By combining the x-ray results with the results on the T_c degradation as a function of the quenching temperature we are now able to give a relation similar to equation (12) for $Ca_3Rh_4Sn_{13}$

$$\Delta T_c/T_{cmax} = 9.8\Delta c_B^\alpha. \tag{13}$$

The degradation of T_c is less sensitive to the number of Sn(I) atoms on the Ca(6) sites in $Ca_3Rh_4Sn_{13}$, than to that of the B atoms on the α sublattice in the case of the A15 compounds. However, note that the degradation of T_c versus the concentration of anti-site defects with respect to the number of atoms per unit cell is found here to be twice that for the A15 compounds, i.e. $\Delta T_c/T_{cmax}$ is 0.67 and 0.35 per per cent of anti-site defects, respectively.

We will now use the above result to obtain more information from our previous experiments on $Ca_3Rh_4Sn_{13}$. In a previous paper (Westerveld *et al* 1987) we reported on the Arrhenius behaviour of the degradation of T_c as a function of the quenching temperature for $Ca_3Rh_4Sn_{13}$. From the slope of the Arrhenius plot we obtained the activation energy (1.16 eV) for the formation of a pair of anti-site defects. However, we were not able to calculate the entropy because of lack of information about the numbers of anti-site defects induced by quenching. This entropy term takes account of the non-configurational entropy contributions involved in the disordering process. Substituting the above results we are now able to calculate this entropy

$$s_a^f/k = 5.3 \pm 0.6. \tag{14}$$

This value for the entropy is twice the value for a pair of anti-site defects in V_3Ga as obtained by Van Winkel *et al* (1984). From this we conclude that the non-configurational entropy changes, for example the vibrational entropy change, due to the anti-site disordering is considerably greater for the ternary $Ca_3Rh_4Sn_{13}$ than for V_3Ga.

We now consider the recovery processes. Upon quenching from high temperatures, thermal vacancies are also induced in the material in addition to pairs of anti-site defects. Let us discuss the results of the annealing experiments on $Ca_3Rh_4Sn_{13}$ in terms of average vacancies with an average formation entropy and enthalpy as we proposed in § 4. In the expression (9) for the recovery of the superconducting transition temperature we observe the occurrence of the ratio $\Delta c(t = 0)/c^v(t = \infty)$ and not the occurrence of $c_v(t)$ alone. As a consequence of this, values for this ratio, obtained from the annealing experiments, only yield values for the average formation enthalpy of the vacancies, but not values for the vacancy formation entropy, which cancel out.

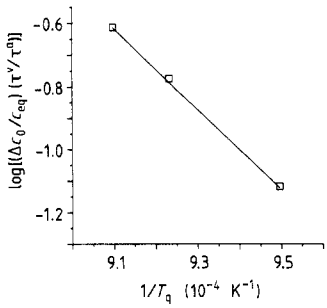

Figure 7. Arrhenius plot of $(\Delta c^v(t=0)/c^v(t=\infty))(\tau^v/\tau^a)$ versus the reciprocal quenching temperature T_q. h^f_{1v} is estimated from the slope of the curve.

From three series of samples, quenched from different temperatures and subsequently annealed at the same intermediate temperature, the vacancy formation enthalpy is obtained.

The data were fitted to the equation (9) with τ^a, τ^v and $\Delta c^v(t=0)/c^v(t=\infty)(\tau^v/\tau^a)$ as the three unknown parameters. Since we performed the recoveries at the same temperature the kinetic parameters τ^a and τ^v are expected not to vary. This was corroborated by the experiment within experimental error. However, the third parameter does vary as a function of quenching temperature, due to the different amounts of vacancies quenched in. In figure 7 this quantity is shown in an Arrhenius plot. From this plot the activation energy for vacancy formation is estimated as

$$h^f_{1v} = 1.1\,\text{eV}. \tag{15}$$

This value is somewhat high in comparison with a value of 0.8 eV estimated by the Miedema model (Miedema and De Châtel 1980). Another estimate can be made on the basis of the melting temperature of the ternary compound by the empirical rule for vacancy formation in pure metals

$$h^f_{1v} = 9kT_m \tag{16}$$

which yields a value of 0.94 eV.

In order to examine the kinetics of the recovery process we also quenched a number of samples from the same high temperature and annealed them at different temperatures. By annealing at different temperatures the activation enthalpy for the vacancy migration and for the anti-site annihilation can be obtained. To keep the experimental error within acceptable limits, the recovery process of the superconducting transition temperature must be followed over a temperature range of at least 2 K. For $Ca_3Rh_4Sn_{13}$ this requires a quenching temperature of 800 °C or higher. However the quenching temperature should be kept as low as possible to measure the tail of the reordering plot with sufficient accuracy. In fact a quenching temperature of 810 °C appeared to be too high to calculate τ^a from the slope of the tail. The three-parameter fits to the isothermal recovery plots following equation (9) yield reliable values for $\Delta c^v(t=0)/c^v(t=\infty)(\tau^v/\tau^a)$ and τ^v but less reliable values for τ^a. Substituting 1.10 eV for the formation enthalpy of the vacancies in $\Delta c^v(t=0)/c^v(t=\infty)$ gives the temperature dependence of this quantity and together with the value of τ^v, τ^a is obtained from $\Delta c^v(t=0)/c^v(t=\infty)(\tau^v/\tau^a)$.

The logarithm of the values of τ^v versus the reciprocal annealing temperature are given in figure 8. From the slope a vacancy migration enthalpy of 0.89 eV is found. The Arrhenius curve for τ^a is plotted in figure 9, with 2.14 eV for the activation energy for the anti-site annihilation process. For the annihilation of the anti-site defects diffusion of the Ca and the Sn atoms from the 'wrong' to the 'right' sublattice is necessary. In a

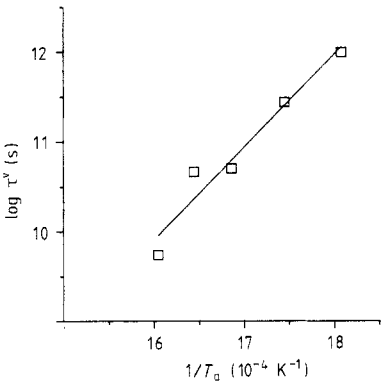

Figure 8. Arrhenius plot of the logarithm of τ^v versus the reciprocal annealing temperature T_a. h^m_{1v} is obtained from the slope of the curve.

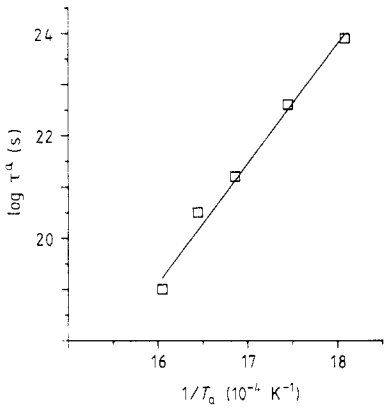

Figure 9. Arrhenius plot of the logarithm of τ^a versus the reciprocal annealing temperature T_a. h^a is obtained from the slope of the curve.

Table 4. Parameters for defect formation and defect kinetics in $Ca_3Rh_4Sn_{13}$ obtained from the annealing experiments.

Vacancy formation	h^f_{1v} (eV) 1.10 ± 0.03
Vacancy migration	h^m_{1v} (eV) 0.89 ± 0.09
	τ^v_0 (s) (1.3 ± 0.2) × 10^{-3}
Anti-site defect annihilation	h^a (eV) 2.14 ± 0.10
	τ^a_0 (s) (9.3 ± 1.7) × 10^{-10}

diffusion model based on average quantities the sum of the formation and the migration energies is equal to the activation energy for diffusion of the atoms. The sum of both activation energies, obtained experimentally, is 1.99 eV and is in fair agreement with the 2.14 eV for the atomic migration calculated directly from the annealing experiments. Also the empirical rule for the activation energy for diffusion in pure metals relative to the melting point seems to hold in the case of this ternary intermetallic compound, namely

$$h^a \simeq 18kT_m = 1.87\,\text{eV}. \tag{17}$$

The results for the activation energies, obtained from the isothermal recovery measurements, can also be compared to the isochronal recovery experiments shown in figure 4. The plateau at 400 °C divides the plot into the two stages of the recovery process. An estimation can be made of the ratio of the activation energies involved in both stages by

$$T_1/T_2 = (h^f_{1v} + h^a)/(h^f_{1v} + h^m_{1v} + h^a) = 0.77 \tag{18}$$

T_1 and T_2 being the annealing temperatures at which the recovery of T_c process occurs most rapidly in the first and the second stages, respectively. This value is in good agreement with the value of 0.79 calculated from the activation energies obtained from the isothermal recovery plots.

In table 4 the parameters describing the defect kinetics obtained by the annealing experiments are listed. The pre-exponential factor found for the vacancy migration is

$\tau_0^v = 1.3 \times 10^{-3}$ s. If we assume that the vacancies migrate to pre-existing dislocation pipes we can make an estimation for the dislocation density from τ_0^v. For this migration to a network of cylindrical pipes, we only have to consider the vacancy diffusion in two dimensions, namely perpendicular to the pipes. We then obtain the mean square displacement for this during an annealing time t

$$\langle R^2 \rangle = 4D_v t \tag{19}$$

where D_v is the diffusion coefficient for vacancies. τ^v is a measure of the time needed for a vacancy to reach a dislocation. So a measure for the dislocation density is

$$d \simeq 1/\langle R^2 \rangle_{t=\tau^v} = 1/4D_v\tau^v. \tag{20}$$

The diffusion coefficient D_v can be expressed in terms of atomistic quantities (Manning 1968)

$$D_v = nr^2/4t = r^2/4\tau \tag{21}$$

where n is the number of jumps during a time t, r the elementary one-jump displacement vector and $\tau = t/n$ the mean time for a vacancy to stay at one lattice site. Taking equation (20) and equation (21) together leads to an approximate expression for d

$$d \simeq \tau/r^2\tau^v \simeq (\nu_0 r^2 \tau_0^v)^{-1} \tag{22}$$

with ν_0 the vibrational frequency of the atoms. Taking $\nu_0 = 10^{13}\,s^{-1}$ and $r = 2$ Å we find for the dislocation density $10^5\,cm^{-2}$. This seems to be a reasonable value for the single crystals obtained by growth from molten metal solution.

From the value of 9.3×10^{-10} s for τ_0^a we may conclude that the reordering of the anti-site defects is clearly not a one-jump process. The number of jumps needed for the reordering of one anti-structure atom is of the order of 10^4. This is a factor of 16 smaller than in the case of V_3Ga (Van Winkel *et al* 1985).

6. Conclusions

In $Ca_3Rh_4Sn_{13}$ the T_c degradation is caused by Ca–Sn(I) anti-site defects. From x-ray occupancy measurements a tentative relation (13) can be obtained between the T_c degradation and the number of anti-site defects.

Reordering of quenched material upon annealing at intermediate temperatures can be described in terms of average vacancy concentration and average jump probabilities. Values were obtained for the vacancy formation energy, the vacancy migration energy and the activation energy for atomic diffusion. These energies correlate with the melting temperature following the well-known empirical relation for pure FCC metals (see table 4).

Acknowledgments

We thank Messrs D Heydenrijk, A C Moleman, B Zwart, H Schlatter and A M Riemersma for their technical assistance, Drs G F Bastin and H J M Heijligers for microprobe analysis. This work was financially supported by the 'Stichting voor Fundamenteel Onderzoek der Materie' (FOM).

References

Bakker H 1987 *Mater. Sci. Forum* **15–18** 1152–82
Bastin G F, Heijligers H J M and van Loo J J 1984a *X-ray Spectrom.* **31** 91
—— 1984b *Scanning* **6** 58
Fähnle M 1982 *J. Low-Temp. Phys.* **46** 3
Flükiger R, Staudenmann J L and Fischer P 1976 *J. Less-Common Met.* **50** 253
Franklin A D 1972 *Point Defects in Solids* vol. 1 ed. J H Crawford Jr, and L M Slifkin (New York: Plenum)
Hall S R and Stewart J M (ed.) 1987 *XTAL2.2 User's Manual* (Universities of Western Australia and Maryland)
Hodeau J L, Chenavas J, Marezio M and Remeika J-P 1980 *Solid State Commun.* **36** 839
Manning J R 1968 *Diffusion Kinetics for Atoms in Crystals* (Princeton: Van Nostrand)
Miedema A R and De Châtel P F 1980 *Theory of Alloy Phase Formation* ed. L H Bennett (Warrendale, USA: Met. Soc. AIME) p 344
Remeika J-P, Espinosa G P, Cooper A S, Barz, H, Rowell J M, McWhan D B, Vandenberg J M, Moncton D E, Fisk Z, Woolf L D, Hamaker H C, Maple M B, Shirane G and Thomlinson W 1980 *Solid State Commun.* **34** 923
Sweedler A R, Snead C L Jr and Cos D E 1976 *Metallurgy of Superconducting Materials* ed. T Luhman and D D Hughes (New York: Academic Press)
Van Winkel A, Weeber A W and Bakker H 1984 *J. Phys. F: Met. Phys.* **14** 2631
Van Winkel A and Bakker H 1985 *J. Phys. F: Met. Phys.* **15** 1565
Walker N and Stuart D 1983 *Acta Crystallogr.* A **39** 158
Waegemaekers A A H J, de Reus R and Bakker H 1988 *Phil. Mag.* **57** 811
Westerveld J P A and Bakker H 1986 *Phil. Mag.* **54** L15
Westerveld J P A, Lo Cascio D M R and Bakker H 1987 *J. Phys. F: Met. Phys.* **17** 1963